Journal of Biomedical Informatics 59 (2016) 240–247

Contents lists available at ScienceDirect

Journal of Biomedical Informatics

journal homepage: www.elsevier.com/locate/yjbin

Analysis of topographical distribution of prostate cancer and related pathological findings in prostatectomy specimens using cMDX document architecture

Okyaz Eminaga [a,*], Axel Semjonow [b], Elke Eltze [c], Olaf Bettendorf [d], Anne Schultheis [e], Ute Warnecke-Eberz [f], Ilgar Akbarov [a], Sebastian Wille [a], Udo Engelmann [a]

[a] Dept. of Urology, University Hospital of Cologne, Kerpener Straße 62, D-50937 Cologne, Germany
[b] Prostate Center, Dept. of Urology, University Hospital Muenster, Albert-Schweitzer-Campus 1, D-48149 Muenster, Germany
[c] Institute for Pathology Saarbrücken-Rastpfuhl, Rheinstrasse 2, D-66113 Saarbrücken, Germany
[d] Institute of Pathology and Cytology, Technikerstrasse 14, D-48465 Schüttorf, Germany
[e] Institute for Pathology, University Hospital of Cologne, Kerpener Straße 62, D-50937 Cologne, Germany
[f] Department for Visceral Surgery, University Hospital Cologne, Kerpener Straße 62, D-50937 Cologne, Germany

ARTICLE INFO

Article history:
Received 2 June 2015
Revised 10 December 2015
Accepted 13 December 2015
Available online 17 December 2015

Keywords:
Zonal anatomy
Spatial distribution
CMDX
Biopsy
Diagnostic tools
Prostate cancer

ABSTRACT

Introduction: Understanding the topographical distribution of prostate cancer (PCa) foci is necessary to optimize the biopsy strategy. This study was done to develop a technical approach that facilitates the analysis of the topographical distribution of PCa foci and related pathological findings (i.e., Gleason score and foci dimensions) in prostatectomy specimens.
Material & methods: The topographical distribution of PCa foci and related pathologic evaluations were documented using the cMDX documentation system. The project was performed in three steps. First, we analyzed the document architecture of cMDX, including textual and graphical information. Second, we developed a data model supporting the topographic analysis of PCa foci and related pathologic parameters. Finally, we retrospectively evaluated the analysis model in 168 consecutive prostatectomy specimens of men diagnosed with PCa who underwent total prostate removal. The distribution of PCa foci were analyzed and visualized in a heat map. The color depth of the heat map was reduced to 6 colors representing the PCa foci frequencies, using an image posterization effect. We randomly defined 9 regions in which the frequency of PCa foci and related pathologic findings were estimated.
Results: Evaluation of the spatial distribution of tumor foci according to Gleason score was enabled by using a filter function for the score, as defined by the user. PCa foci with Gleason score (Gls) 6 were identified in 67.3% of the patients, of which 55 (48.2%) also had PCa foci with Gls between 7 and 10. Of 1173 PCa foci, 557 had Gls 6, whereas 616 PCa foci had Gls > 6. PCa foci with Gls 6 were mostly concentrated in the posterior part of the peripheral zone of the prostate, whereas PCa foci with Gls > 6 extended toward the basal and anterior parts of the prostate. The mean size of PCa foci with Gls 6 was significantly lower than that of PCa with Gls > 6 ($P < 0.0001$).
Conclusion: The cMDX-based technical approach facilitates analysis of the topographical distribution of PCa foci and related pathologic findings in prostatectomy specimens.

1. Introduction

Prostate cancer (PCa) remains the most-diagnosed cancer in men [1], and a majority of these patients undergo total prostate removal (radical prostatectomy) [2]. The diagnosis of PCa is regularly confirmed by prostate needle biopsy. However, there is a risk of missing PCa foci in needle biopsy, especially those located in the anterior part of the prostate [3–5]. Rocco et al. concluded that the sensitivity of double sextant biopsy for diagnosing clinically significant PCa was 75% [3]. Another study found that PCa foci missed by biopsy were clinically significant in 40% of patients [5]. Furthermore, the cancer detection rate with repeat biopsies varies from 10% to 20% [6]. The detection rate of prostate cancer with prostate biopsy remains a central issue in urological oncology.

* Corresponding author. Tel.: +49 221 478 0.
E-mail address: okyaz.eminaga@uk-koeln.de (O. Eminaga).

http://dx.doi.org/10.1016/j.jbi.2015.12.009
1532-0464/

Understanding the topographical distribution of PCa foci is necessary to optimize the biopsy strategy.

The histopathological evaluation of prostatectomy specimens is essential for decision-making and for predicting a patient's outcome [7]. Consequently, diverse standardized sectioning and documentation protocols for radical prostatectomy specimens have been developed [7–9]. We applied a standardized protocol for pathological reports according to Bettendorf et al. [9] (Fig. 1). Each report contains personal data and clinical data (tumor classification, grading, and malignancy) and a diagrammatic representation of the histopathological findings in the prostate. This morphometrical diagram of the prostate enables documentation of tumor-extension patterns and the status of the surgical margins in radical prostatectomy specimens. Additionally, an approximate estimation of the absolute and relative tumor volumes is feasible using this diagram [9,10]. Tumor volume is assumed to be an independent predictor for biochemical recurrence in men with PCa after radical prostatectomy [11].

The purpose of this article is to introduce a technical approach to facilitate analysis of the topographical distribution patterns of PCa foci and related pathological findings (Gleason score and foci dimensions) in prostatectomy specimens. The technical approach is based on cMDX© (Clinical Map Document based on XML), which is open source, meets Open Packaging conventions, and provides a data-acquisition model for graphical and textual clinical information. The graphical information is stored using a method based on scalable vector graphics. cMDX has already been applied in the reporting and analysis of PCa foci in prostatectomy specimens [10].

In this context, the topographical distribution of PCa foci and related pathologic findings were evaluated using the cMDX documentation system [10,12]. Furthermore, we evaluated the distribution of PCa foci in relation to their location within the prostate. Our aim is to provide a technical approach to enable analysis of the distribution of PCa foci in order to support studies related to prostate biopsy and investigating diagnostic approaches to improve detection rates in men with suspected PCa.

2. Materials and methods

The current study was performed by the Department of Urology at the University Hospital of Cologne between February 2012 and March 2013. The study was performed within the scope of investigating the distribution of Gleason scores within prostates affected by PCa. The Gleason score represents the microscopic appearance of the prostate cancer and is associated with the prognosis. The topographical distribution of PCa and related pathologic evaluations were documented using the cMDX documentation system [10,12]. The project was performed in three steps. First, we analyzed the document architecture of cMDX, including textual and graphical information. Second, we developed an evaluation model supporting the topographic analysis of PCa foci and related pathologic parameters. Finally, we evaluated the analysis model in 168 consecutive prostatectomy specimens of men with diagnosed with PCa who underwent total prostate removal. The surgical treatments were performed by the Department of Urology at the University Hospital of Cologne between 2008 and 2012. We retrospectively evaluated all prostatectomy specimens. A pathologist (A.S.) performed the pathological evaluations.

2.1. Analysis of document architecture

The cMDX document architecture consists of two types of content: patient-related data and template data (Fig. 2), as described in our recent study [10]. Template data describe the anatomical prostate schema designed by Bettendorf et al. and stored in "Mask.xml." In addition, an XML document named "Tools.xml" stores information defining drawing tools applied to sketch pathological changes in scheme styles (e.g., freehand drawing) and provides parameters for the drawing tools [10].

The patient data consisted of two types of information. The first was morphometrical information about histological changes (PCa, high-grade prostatic intraepithelial neoplasia [HGPIN], and positive surgical margins) with additional textual descriptions (Gleason score, length of positive surgical margins). Each PCa focus was related to pathologic findings (Gleason score and tumor volume percentage). The second type of information was clinical and personal data in text form. Consequently, there are two XML containers: "Form.xml" and "Map.xml." "Map.xml" captures morphometrical information about histological findings to reconstruct them in schematic styles. The representation of the spread pattern of PCa was based on vector graphics. An XML element called "Befund" was integrated into the CDATA-Section of a graphic object showing a PCa focus. "Befund" captured information about the histological patterns of the corresponding PCa focus. Form.xml contained the element "Formular" with attributes containing pathological findings and personal data. Pathological findings were textual information not directly related to the morphometrical data. Sensitive personal data were encrypted with Rijndael 256-bit cryptography to avoid misuse.

2.2. Development of a cMDX-based analysis model for topographic analysis

The following elements are required to develop a cMDX-based data analysis model. First, the graphical information about the tumor foci with the corresponding textual data (e.g. Gleason score and tumor size) is stored in the electronic report. Second, a background layout contains graphical and textual information about the prostate slices. Third, a filter layout defines the regions of interest. Fourth, a search function to filter tumor foci meets the criteria (e.g. Gleason score). Finally, a data-acquisition model is applied to store the results for further analysis. The results should be transferable to common analysis software. In cMDX document architecture, the XML document "Map.xml" includes graphical information about PCa foci with related pathological findings that are required for topographical analysis. The XML document "Mask.xml" defines the schematic diagram of the prostate gland. Therefore, we focused on "Map.xml" and "Mask.xml" to integrate cMDX into a data analysis model.

The data analysis model should facilitate analysis of the spatial distribution of PCa foci and their pathological features inside the prostate, as well as the generation of a heat map that represents the distribution of PCa foci. Moreover, the model should enable division of the prostate into regions of interest to analyze the presence status, frequency, and density of PCa foci in each region of interest. For these purposes, we constructed three possible workflows of topographic analysis, as shown in Fig. 3. The first workflow evaluated the association between pathologic findings (i.e. HGPIN and PCa). The second workflow investigated the probability and frequency of PCa foci present in defined regions of interest in the prostate. The third workflow focused on tumor foci meeting the search criteria (i.e. Gleason score) and investigated the probability and frequency of the selected tumor foci in defined regions. The Gleason score was divided into four groups: 6, 7a (3 + 4), 7b (4 + 3), and 8–10. Several authors have stated that Gls 7b was associated with poorer clinical outcomes than Gls 7a [13,14].

To realize the analysis model, we designed a four-layer data model based on cMDX, as shown in Fig. 4. The first layer defined the background and the schematic diagram of the prostate and required information provided by a cMDX template (Supplement

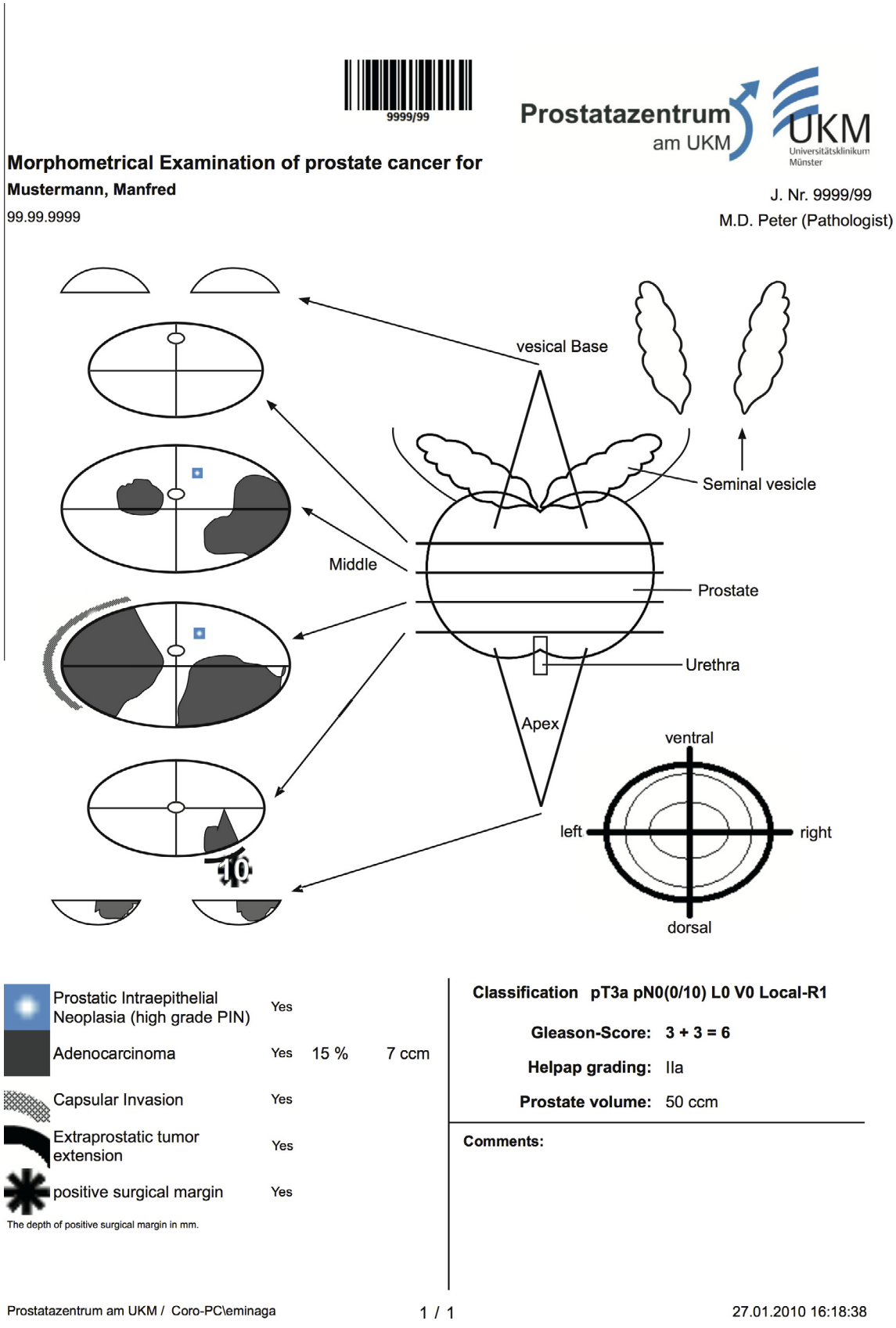

Fig. 1. An example of a pathological report including a diagrammatic representation of the histopathological findings in the prostate, and an example of a morphometric mapping of a radical prostatectomy specimen showing an adenocarcinoma of the prostate in the left lobe with extracapsular tumor extensions and a positive surgical margin. In addition to the Gleason system, the tumors are graded according to Helpap. Here, prostate cancer takes up about 15% of the total area of the prostate, which corresponds to an estimated tumor volume of 7.5 cm^3 in a prostate of 50 cm^3. The computational estimation of tumor volume was performed as previously described by Eminaga et al. [10].

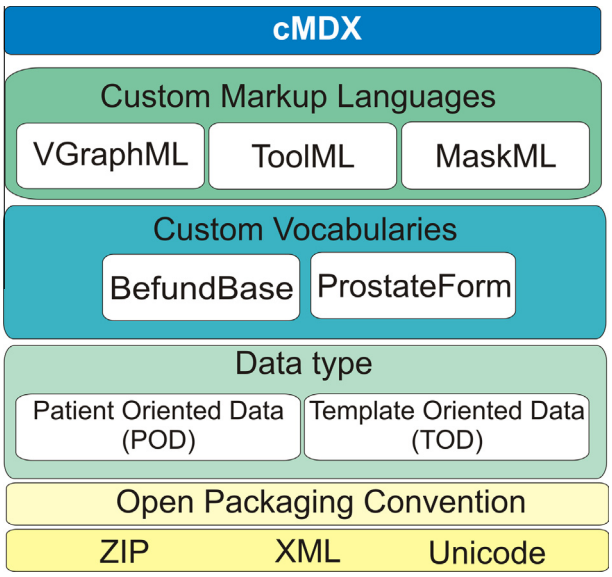

Fig. 2. The components of the cMDX document architecture.

file 1). The second layer contained graphical data defining regions of interest in the prostate stored in a cMDX document (Supplement file 2). The third layer included information about the PCa foci with related pathological findings obtained from cMDX-based pathologic reports (Supplement file 3). The fourth layer showed the results of topographical analysis in a heat map or pixel array (Supplement files 4 & Fig. 6).

The 4-layer data model and filter function were integrated into a cMDX Analyzer tool (Supplement file 5) and the incidence of PCa was determined for each slice. A pixel grid was generated for each slice to calculate the cumulative frequency of PCa foci (Supplement file 6). When the filter function was applied, only PCa foci intersecting with the regions of interest were considered for topographical analysis (Fig. 5). Multiple filters can be defined by the user to determine the frequency of PCa in the region of interest. A heat map was generated to represent the PCa distribution, which can be saved in an image file format. The color gradient represents the frequency of PCa in each pixel (red: highest frequency; blue: lowest frequency). The cumulative frequency of PCa for each pixel located in the region was calculated in parallel. A list containing the tumor-volume percentage and the Gleason score of every PCa focus in each slice or region of interest was generated. The results of the distribution analysis were saved in the CSV (comma-separated values) file format. The resulting data were exported into R (R Foundation for Statistical Computing, Vienna, Austria) to determine the geometric mean frequency of PCa per pixel, region, or slice. The density of PCa foci per region was calculated by dividing the geometric mean frequency of PCa into the number of prostatectomy specimens included in the distribution analysis. The median, range, and 95% confidence interval (CI) of the PCa frequency were also calculated.

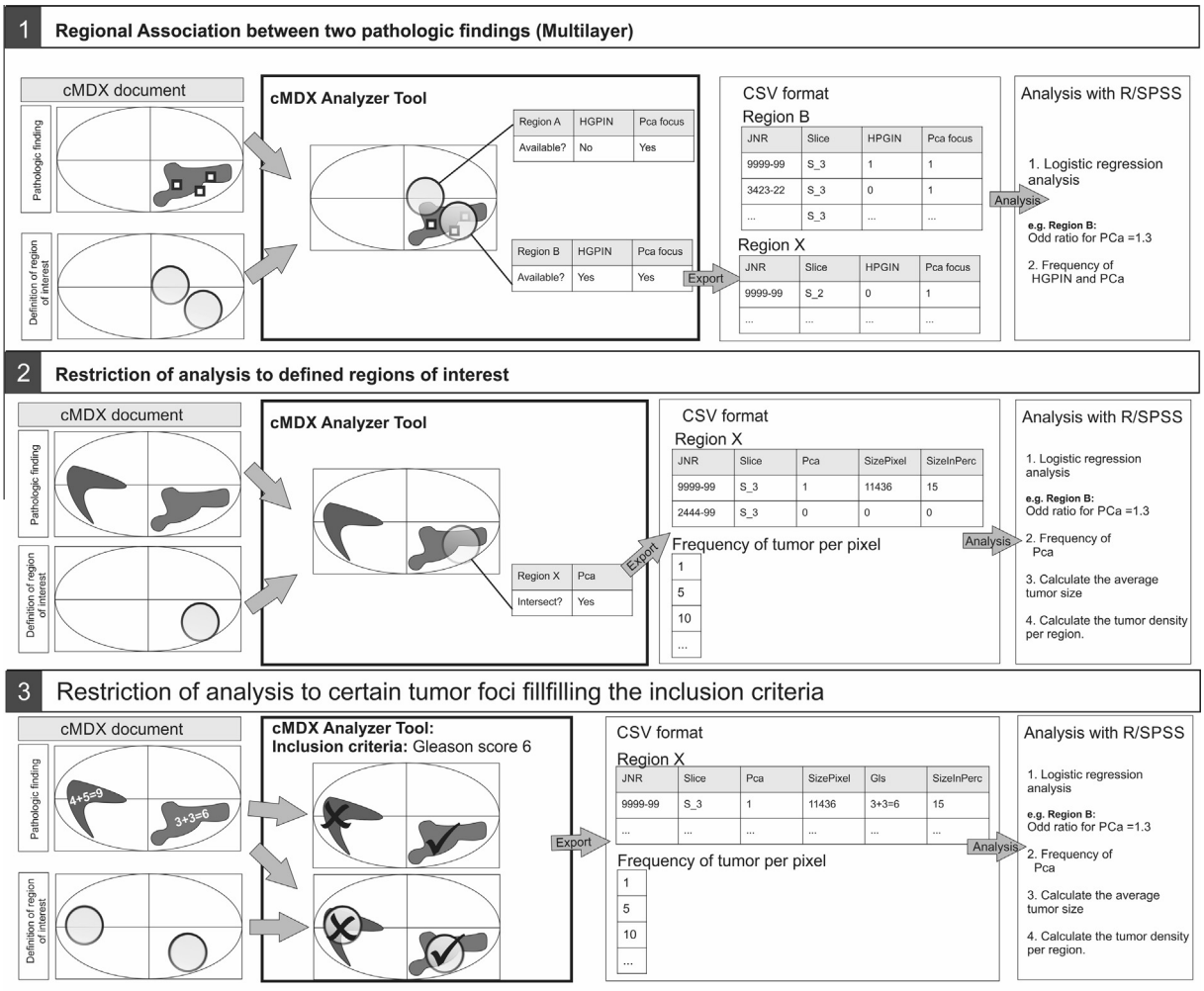

Fig. 3. The diagram illustrated the work follow to analyze the spatial distribution of PCa foci.

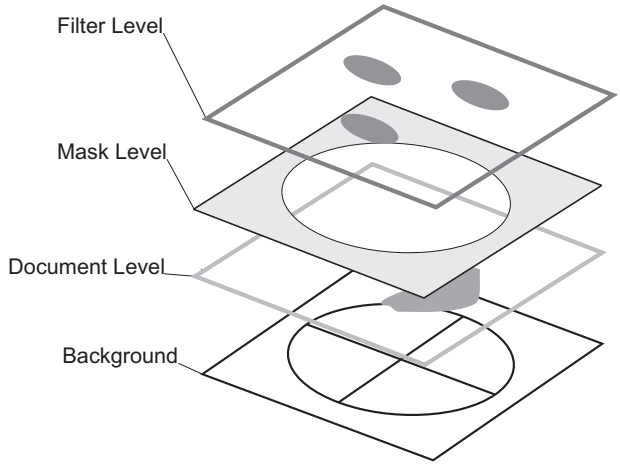

Fig. 4. Four-layer visualization model. Workflow: (1) The filter layer registers pixels affected by prostate cancer in regions of interest defined by the filter function. (2) The mask layer defines the schematic diagrams. (3) The document layer represents the graphical information from the cMDX document. (4) The background layer contains background images with graphical descriptions.

2.3. Evaluation of the analysis model

The cMDX pathology reports of 168 consecutive prostatectomy (total prostate removal) specimens of men diagnosed with PCa were considered for evaluation and validation of the data analysis model. All prostatectomy specimens were retrospectively evaluated as described elsewhere [10]. The cMDX tool was used to analyze the distribution of PCa and its related pathological parameters. The topographical distribution of the tumor foci in the prostate was evaluated according to Gleason score and was presented as a heat map. The color density of the heat map was reduced to six colors in order to distinguish regions with different PCa frequencies by using the image-posterization effect provided by the image-processing software Paint.NET. After posterization, we focused on regions showing one of the top three frequency classes of PCa (red, yellow, or green; Fig. 6). We randomly defined nine regions of interest inside the prostate and generated corresponding cMDX documents using the cMDX Editor tool. To rollout a systematic error by analyzing, we matched the distribution pattern of the PCa foci to the heat map to determine the precision of the spatial localizations of the foci for each of the 20 prostatectomy specimens that were randomly selected. The locations of the PCa foci on the heat map were evaluated in comparison to the original reports before and after defining the region of interest. The precision was calculated by dividing the number of intersected pixels into the number of all pixels affected by PCa, and the duration of analysis was estimated.

3. Results

The analysis tool could successfully evaluate the spatial distribution of 168 prostatectomy specimens. The analysis of these cMDX reports took 12 ± 2 seconds per filter. To evaluate the memory stability of the analysis tool, these filters were multiplexed up to 1000, and the analysis was repeated 1000 times. The evaluation of the spatial distribution of tumor foci according to their Gleason scores was made feasible by using the filter function for the Gleason score as defined by the user (Fig. 5). Data related to the surface size (given as percentage), the slice location, and the Gleason scores of all of the tumor foci were generated and stored in a CSV format and imported into statistical software, such as SPSS and R.

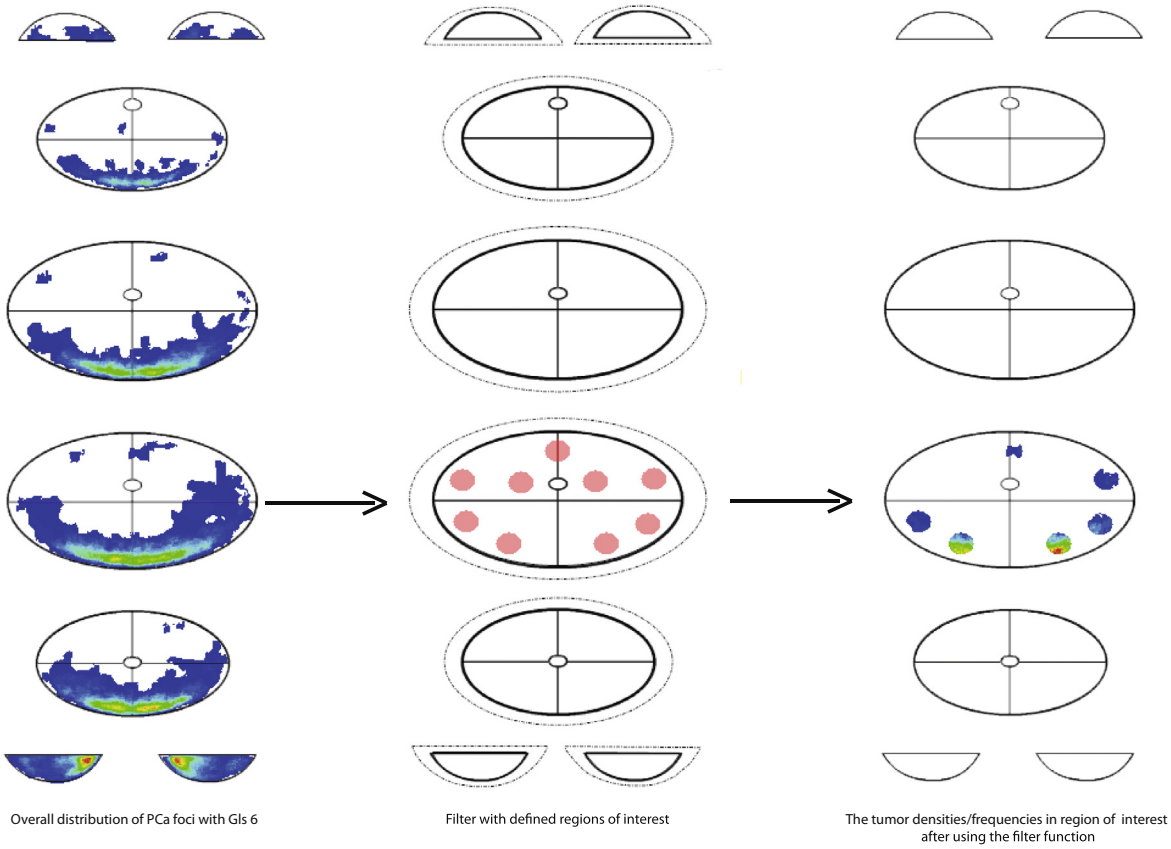

Fig. 5. The result of the topographical analysis before and after applying the filter function.

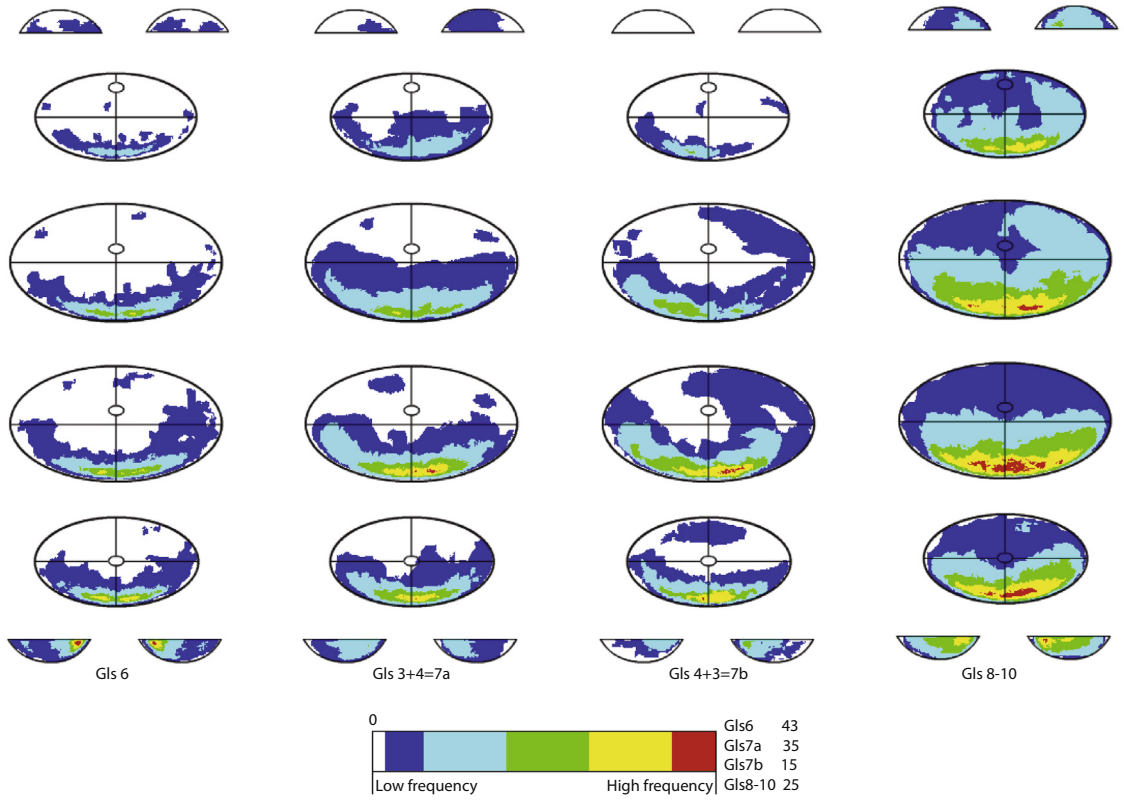

Fig. 6. Distribution of prostate cancer according to Gleason Score. The frequency of tumor foci in the various locations are coded by colors: blue = low frequency, red = high frequency. (For interpretation of the references to colour in this figure legend, the reader is referred to the web version of this article.)

The acquired data was directly analyzable (Supplement file 6). The implementation of the regional filter function enabled the evaluation of tumor foci using the criteria defined by the user to assist in determining the probability of tumor existence based on certain pathological features in the defined regions. The criteria consisted of the Gleason score and the availability of tumor foci in the regions of interest. The user can define regions of interest by drawing them on the schematic diagram of the prostate using the cMDX Editor. A list of journal numbers for specimens with tumor foci in these regions was generated. Using the journal numbers as a reference key enabled the merging lists from different regions into a single table in R. The accuracy and precision analysis showed that all pixels of tumor foci intersecting with the defined regions were captured in 20 cases, even after repeating the analysis three times.

The cMDX Editor was used to digitize 168 reports of radical prostatectomy specimens. The computerized estimation showed that the mean tumor volume was 7.5 cm^3 (95% CI: 5.8–9.2). The median age of the patients was 65 years at the time of prostatectomy. Overall, most of the PCa foci were localized in the peripheral zone of the apical half of the prostate. The frequency of PCa was lower in the basal half of the prostate in comparison to the apical half. PCa foci with Gls 6 were identified in 67.3% of the patients ($n = 114$). Among these patients (48.2%), 55 also had PCa foci with Gls between 7 and 10. Of 1173 PCa foci, 557 had Gls 6, whereas 616 PCa foci had Gls > 6. PCa foci with Gls 6 were mostly concentrated in the posterior part of the peripheral zone of the prostate, whereas PCa foci with Gls > 6 extended toward the basal and anterior parts of the prostate (Fig. 6). The mean size of PCa foci with Gls 6 (0.340% of the slice size; 95% CI: 0.30–0.39) was significantly lower than those with Gls > 6 (2.1% of the slice size, 95% CI: 1.4–2.9) ($P < 0.0001$). The odds ratio (OR) of the co-existence of a Gls 6 PCa (OR: 1.696; 95% CI: 0.839–3.428; $P = 0.140$) was higher in PCa foci with Gls 3 + 4 = 7 but not significantly, whereas OR for the co-existence of Gls 6 PCa foci was significantly lower in foci with Gls 4 + 3 = 7 and Gls 8–10 (OR: 0.196, 95% CI: 0.060–0.200; $P < 0.0001$). In the regions of interest, we observed a variation in the presence of PCa foci with Gls 3 + 3 = 6, between 27.9% and 47.0%. PCa foci with Gls 7a (3 + 4) were found at frequencies between 32.1% and 11.1%. The frequency of PCa foci with Gls 7b (4 + 3) ranged between 11.0% and 7.10%. PCa foci with Gls 8–10 was observed at a frequency ranging between 16.7% and 19.0% of the total cases.

4. Discussion

Applying the cMDX documentation system facilitates analysis of the spatial distribution of PCa foci and related pathological findings. The size and location of each PCa focus can be determined, and the volume estimation of the PCa foci can be calculated based on Bettendorf's scheme [9]. The spatial distribution of PCa foci can be studied to optimize biopsy schemes or to analyze areas of the prostate missed by conventional biopsies [3–5].

Sinnott et al. reported that PCa foci missed by biopsy were clinically significant in 40% of patients [5]. Djavan et al. reported that the cancer-detection rate on repeat biopsy varies from 10% to 20% [6]. The indication for repeat biopsies should be critically discussed. One in ten men refuse a repeat biopsy or require sedation or analgesia due to pain, complications, and discomfort [15]. Therefore, researchers continue to develop strategies to improve prostate biopsy detection rates and staging information. We successfully performed two studies investigating the topographical association between PCa and HGPIN (a presumable precursor of PCa) and the prognostic significance of the location of extracapsular extensions or positive surgical margins in men with PCa, based on the cMDX analysis system [16,17]. In addition, we could

evaluate the spatial distribution of PCa foci according to PSA levels and identified that anterior tumors were frequent with increasing PSA levels [18]. Furthermore, we investigated the spatial distribution of Gleason scores within the prostate to understand the pathogenesis of PCa. Our findings confirm previous general descriptions of the location of PCa foci inside the prostate [19,20].

Many computational approaches have been developed to reconstruct the spatial distribution of PCa [20–24]. These methods enable the 3D reconstruction of PCa foci and were developed to optimize the biopsy schema. For instance, Chen, Mazal, and Narayanan evaluated the spatial distribution of PCa by using a 3D reconstruction model of the prostate to optimize the biopsy schema [20–22]. Additionally, Rojas et al. developed a 3D reconstruction of PCa to generate a spatial distribution of PCa foci inside the prostate and to evaluate the spatial distribution according to clinical features such as PSA level and age at diagnosis [25]. However, none of these methods can analyze the spatial distribution of Gleason scores within the prostate gland. Different Gleason patterns can be found in a single prostatectomy specimen. The Gleason score consists of the two patterns most often observed in a tumor focus. The final pathology report includes the most-observed Gleason score in the prostatectomy specimen. Therefore, a single tumor focus with a higher Gleason score is not documented in the final report if PCa foci with low Gleason scores are more frequent. There are indications that the tertiary Gleason pattern may influence the clinical outcome and should be included in the final pathology report [26,27]. Our approach can document all Gleason patterns observed in the prostatectomy specimens and evaluate the spatial distribution of Gleason scores. The spatial distribution of Gleason scores is valuable for a better understanding of the upgrading of a Gleason score of 6. A Gleason score of 6 at biopsy is one of the criteria for active surveillance as a treatment option in patients with low-risk PCa. Understanding the spatial distribution of Gleason scores is necessary to minimize the risk of Gleason score upgrading by identifying regions of the prostate associated with an increased risk for such upgrading. In our collective sample, Gleason score upgrading was observed in prostatectomy specimens in 45.5% of PCa cases with a Gleason score of 6 determined on prostate biopsy. Similar results have been reported in other studies [28–30].

The computational reconstruction of PCa foci and the prostate is time-intensive and expensive, making it unsuitable for routine clinical use. All 3D-based reconstruction models are time- and cost-intensive and require technical abilities that are not available at most pathology institutes. A recent study concluded that the cMDX system is suitable for the documentation of pathological examinations of prostatectomy specimens and can be integrated into the clinical routine [12]. In addition, the cMDX documentation system enables analyses of the spatial distributions of PCa foci, extracapsular extensions, and positive surgical margins, which are visualized on a heat map without any major preparation. Extracapsular extensions and positive surgical margins are not considered in other computational methods [20–24]. The status of the surgical margins plays an essential role in clinical decision-making and quality-management assessments, which are important conditions for the certification of prostate centers [31]. The cMDX documentation system facilitates the extraction of clinical and pathological data collected in the clinical routine, with respect for privacy regulations [12].

We were able to evaluate the distribution of PCa foci and Gleason scores in defined regions by setting filters generated by the cMDX Editor; 1000 filters can be applied by the analysis of the spatial distribution of PCa foci and Gleason scores without the loss of stability of the analysis tools. The Gleason score for each PCa focus was assessed three times to avoid systematic errors. Using these filters enabled the estimation of the frequency and density of PCa foci in defined regions.

Future work will be done to develop a computational approach to generating a 3D reconstruction of the prostate with the spatial distribution of PCa foci based on the cMDX documentation system. We also plan to integrate genetic data into the cMDX document architecture. The cMDX document architecture is extensible and facilitates the integration of additional data for corresponding tumor foci [10].

5. Limitations

This study focused primarily on the development of a tool to enable the analysis of the spatial distribution of PCa in prostatectomy specimens. The transferability of the cMDX analysis system to other clinical fields is therefore limited. The technical approach described here may be accompanied by technical failures, which require appropriate handling to keep the system working without interruption. The cMDX system is still being developed and may require further enhancements in the future.

6. Conclusion

The cMDX system facilitates the analysis of the spatial distribution of PCa and related pathological findings. The applied technique supports a focus on certain regions of the prostate by setting filters in the cMDX analyzer tool. Therefore, the analysis of spatial distribution based on the cMDX documentation system can be applied for research purposes.

Disclosure

No conflict of interest, No financial and material support.

Appendix A. Supplementary material

Supplementary data associated with this article can be found, in the online version, at http://dx.doi.org/10.1016/j.jbi.2015.12.009.

References

[1] A. Jemal, R. Siegel, J. Xu, E. Ward, Cancer statistics, 2010, CA Cancer J. Clin. 60 (5) (2010) 277–300.
[2] F. Abdollah, M. Sun, R. Thuret, C. Jeldres, Z. Tian, A. Briganti, S.F. Shariat, P. Perrotte, P. Rigatti, F. Montorsi, et al., A competing-risks analysis of survival after alternative treatment modalities for prostate cancer patients: 1988–2006, Eur. Urol. 59 (1) (2011) 88–95.
[3] B. Rocco, O. de Cobelli, M.E. Leon, M. Ferruti, M.G. Mastropasqua, D.V. Matei, G. Gazzano, F. Verweij, E. Scardino, G. Musi, et al., Sensitivity and detection rate of a 12-core trans-perineal prostate biopsy: preliminary report, Eur. Urol. 49 (5) (2006) 827–833.
[4] S.R. Bott, M.P. Young, M.J. Kellett, M.C. Parkinson, Contributors to the UCLHTRPD, Anterior prostate cancer: is it more difficult to diagnose?, BJU Int 89 (9) (2002) 886–889.
[5] M. Sinnott, S.M. Falzarano, A.V. Hernandez, J.S. Jones, E.A. Klein, M. Zhou, C. Magi-Galluzzi, Discrepancy in prostate cancer localization between biopsy and prostatectomy specimens in patients with unilateral positive biopsy: implications for focal therapy, Prostate (2011).
[6] B. Djavan, A.R. Zlotta, S. Ekane, M. Remzi, G. Kramer, T. Roumeguere, M. Etemad, R. Wolfram, C.C. Schulman, M. Marberger, Is one set of sextant biopsies enough to rule out prostate Cancer? Influence of transition and total prostate volumes on prostate cancer yield, Eur. Urol. 38 (2) (2000) 218–224.
[7] J.I. Epstein, J. Srigley, D. Grignon, P. Humphrey, Recommendations for the reporting of prostate carcinoma: association of directors of anatomic and surgical pathology, Am. J. Clin. Pathol. 129 (1) (2008) 24–30.
[8] J.R. Srigley, M.B. Amin, D.G. Bostwick, D.J. Grignon, M.E. Hammond, Updated protocol for the examination of specimens from patients with carcinomas of the prostate gland: a basis for checklists. Cancer Committee, Arch. Pathol. Lab. Med. 124 (7) (2000) 1034–1039.
[9] O. Bettendorf, F. Oberpenning, T. Kopke, A. Heinecke, L. Hertle, W. Boecker, A. Semjonow, Implementation of a map in radical prostatectomy specimen allows visual estimation of tumor volume, Eur. J. Surg. Oncol. 33 (3) (2007) 352–357.
[10] O. Eminaga, R. Hinkelammert, A. Semjonow, J. Neumann, M. Abbas, T. Koepke, O. Bettendorf, E. Eltze, M. Dugas, Clinical map document based on XML

(cMDX): document architecture with mapping feature for reporting and analysing prostate cancer in radical prostatectomy specimens, BMC Med. Inform. Decis. Mak. 10 (2010) 71.
[11] M.A. Uhlman, L. Sun, D.A. Stackhouse, A.A. Caire, T.J. Polascik, C.N. Robertson, J. Madden, R. Vollmer, D.M. Albala, J.W. Moul, Tumor volume, tumor percentage involvement, or prostate volume: which is predictive of prostate-specific antigen recurrence?, Urology 75 (2) (2010) 460–466
[12] O. Eminaga, M. Abbas, R. Hinkelammert, U. Titze, O. Bettendorf, E. Eltze, E. Ozgur, A. Semjonow, CMDX(c)-based single source information system for simplified quality management and clinical research in prostate cancer, BMC Med. Inform. Decis. Mak. 12 (2012) 141.
[13] D.V. Makarov, H. Sanderson, A.W. Partin, J.I. Epstein, Gleason score 7 prostate cancer on needle biopsy: is the prognostic difference in Gleason scores 4 + 3 and 3 + 4 independent of the number of involved cores?, J Urol. 167 (6) (2002) 2440–2442.
[14] A. Amin, A. Partin, J.I. Epstein, Gleason score 7 prostate cancer on needle biopsy: relation of primary pattern 3 or 4 to pathological stage and progression after radical prostatectomy, J. Urol. 186 (4) (2011) 1286–1290.
[15] H. Seymour, M.J. Perry, C. Lee-Elliot, D. Dundas, U. Patel, Pain after transrectal ultrasonography-guided prostate biopsy: the advantages of periprostatic local anaesthesia, BJU Int. 88 (6) (2001) 540–544.
[16] O. Eminaga, R. Hinkelammert, U. Titze, M. Abbas, E. Eltze, O. Bettendorf, A. Semjonow, The presence of positive surgical margins in patients with organ-confined prostate cancer results in biochemical recurrence at a similar rate to that in patients with extracapsular extension and PSA</=10ng/ml, Urol. Oncol. (2013).
[17] O. Eminaga, R. Hinkelammert, M. Abbas, U. Titze, E. Eltze, O. Bettendorf, A. Semjonow, High-grade prostatic intraepithelial neoplasia (HGPIN) and topographical distribution in 1,374 prostatectomy specimens: existence of HGPIN near prostate cancer, Prostate (2013).
[18] O. Eminaga, R. Hinkelammert, M. Abbas, F. Wotzel, E. Eltze, O. Bettendorf, M. Boegemann, A. Semjonow, Preoperative serum prostate-specific antigen levels vary according to the topographical distribution of prostate cancer in prostatectomy specimens, Urology 86 (4) (2015) 798–804.
[19] J.E. McNeal, E.A. Redwine, F.S. Freiha, T.A. Stamey, Zonal distribution of prostatic adenocarcinoma. Correlation with histologic pattern and direction of spread, Am. J. Surg. Pathol. 12 (12) (1988) 897–906.
[20] M.E. Chen, D.A. Johnston, K. Tang, R.J. Babaian, P. Troncoso, Detailed mapping of prostate carcinoma foci: biopsy strategy implications, Cancer 89 (8) (2000) 1800–1809.
[21] P.R. Mazal, A. Haitel, C. Windischberger, B. Djavan, R. Sedivy, E. Moser, M. Susani, Spatial distribution of prostate cancers undetected on initial needle biopsies, Eur. Urol. 39 (6) (2001) 662–668.
[22] R. Narayanan, P.N. Werahera, A. Barqawi, E.D. Crawford, K. Shinohara, A.R. Simoneau, J.S. Suri, Adaptation of a 3D prostate cancer atlas for transrectal ultrasound guided target-specific biopsy, Phys. Med. Biol. 53 (20) (2008) N397–N406.
[23] Z. Yiqiang, S. Dinggang, Z. Jianchao, S. Leon, G. Fichtinger, J. Moul, C. Davatzikos, Targeted prostate biopsy using statistical image analysis, IEEE Trans. Med. Imaging 26 (6) (2007) 779–788.
[24] D. Shen, Z. Lao, J. Zeng, W. Zhang, I.A. Sesterhenn, L. Sun, J.W. Moul, E.H. Herskovits, G. Fichtinger, C. Davatzikos, Optimized prostate biopsy via a statistical atlas of cancer spatial distribution, Med. Image Anal. 8 (2) (2004) 139–150.
[25] K.D. Rojas, M.L. Montero, J. Yao, E. Messing, A. Fazili, J. Joseph, Y. Ou, D.J. Rubens, K.J. Parker, C. Davatzikos, et al., Methodology to study the three-dimensional spatial distribution of prostate cancer and their dependence on clinical parameters, J. Med. Imaging (Bellingham) 2 (3) (2015) 037502.
[26] M. Adam, A. Hannah, L. Budaus, T. Steuber, G. Salomon, U. Michl, A. Haese, M. Fisch, C. Wittmer, S. Steurer, et al., A tertiary Gleason pattern in the prostatectomy specimen and its association with adverse outcome after radical prostatectomy, J. Urol. 192 (1) (2014) 97–101.
[27] J.I. Epstein, Z. Feng, B.J. Trock, P.M. Pierorazio, Upgrading and downgrading of prostate cancer from biopsy to radical prostatectomy: incidence and predictive factors using the modified Gleason grading system and factoring in tertiary grades, Eur. Urol. 61 (5) (2012) 1019–1024.
[28] K.T. Dinh, B.A. Mahal, D.R. Ziehr, V. Muralidhar, Y.W. Chen, V.B. Viswanathan, M.D. Nezolosky, C.J. Beard, T.K. Choueiri, N.E. Martin, et al., Incidence and predictors of upgrading and up staging among 10,000 contemporary patients with low risk prostate cancer, J. Urol. 194 (2) (2015) 343–349.
[29] H. Sarici, O. Telli, O. Yigitbasi, M. Ekici, B.C. Ozgur, C.N. Yuceturk, M. Eroglu, Predictors of Gleason score upgrading in patients with prostate biopsy Gleason score </=6, Can. Urol. Assoc. J. 8 (5–6) (2014) E342–E346.
[30] K.H. Kim, S.K. Lim, T.Y. Shin, J.Y. Lee, B.H. Chung, K.H. Rha, S.J. Hong, Upgrading of Gleason score and prostate volume: a clinicopathological analysis, BJU Int. 111 (8) (2013) 1310–1316.
[31] G.D. Grossfeld, V.S. Tigrani, D. Nudell, M. Roach 3rd, V.K. Weinberg, J.C. Presti Jr., E.J. Small, P.R. Carroll, Management of a positive surgical margin after radical prostatectomy: decision analysis, J. Urol. 164 (1) (2000) 93–99. discussion 100.